Ocean Systems Engineering, *Vol. 10, No. 3 (2020) 289-316*
DOI: https:// doi.org/10.12989/ose.2020.10.3.289

Numerical investigation of the effect of the location of stern planes on submarine wake flow

Shokrallah M. Beigi[1], Alireza Shateri[*1] and Mojtaba D. Manshadi[2b]

[1]*Department of Mechanical Engineering, Engineering Faculty of Shahrekord University, Shahrekord, Iran*
[2]*Department of Mechanical Engineering, Malek Ashtar University, Esfahan, Iran*

(Received January 15, 2020, Revised March 19, 2020, Accepted July 21, 2020)

Abstract. In the present paper, the effect of the location of stern planes on the flow entering the submarine propeller is studied numerically. These planes are mounted on three longitudinal positions on the submarine stern. The results are presented considering the flow field characteristics such as non-dimensional pressure coefficient, effective drag and lift forces on the stern plane, and the wake flow formed at the rear of the submarine where the propeller is located. In the present study, the submarine is studied at fully immersed condition without considering the free surface effects. The numerical results are verified with the experimental data. It is concluded that as the number of planes installed at the end of the stern section along the submarine model increases, the average velocity, width of the wake flow and its turbulence intensity formed at the end of the submarine enhance. This leads to a reduction in the non-uniformity of the inlet flow to the propulsion system.

Keywords: numerical simulation; submarine model; stern planes; displacement; wake flow

1. Introduction

Submarine is an underwater vehicle that includes the main hull and various appendages. The flow field around its main hull with no angle of attack does not show flow separation and vortex formation. However, when other appendage parts are mounted on the hull, the shape of the streamlines is greatly influenced by the shape of the hull, leading to the formation of a complex flow field around it. Wake flow behind the submarine hull has a significant effect on its performance. The fluid flow passes over the submarine model comprises a horseshoe vortex at the sail junction to the hull, a pair of sail tip vortices, sail wake flow, and a complex flow structure resulting from the interaction between wake flows and vortex structures generated by fins. Horseshoe vortex is a vortex system that creates a complex flow in encountering with the boundary layer flow and reaches the propeller. Just before the propeller, both horseshoe and stern planes tip vortices are produced at the stern for each fin. This thick wake is created by the reverse pressure gradient induced by surface change at the submarine's heel. Fig. 1 shows the schematic of the vortex structures formed on the submarine body due to the presence of appendages. These vortex structures are created by the

∗Corresponding author, Associate professor, E-mail: shateri@eng.sku.ac.ir
[a] Ph.D. Student, E-mail: shbeigi.2478@gmail.com
[b] Associate Professor, E-mail: dehghanmanshadi@gmail.com

 ISSN: 2093-6702 (Print), 2093-677X (Online)

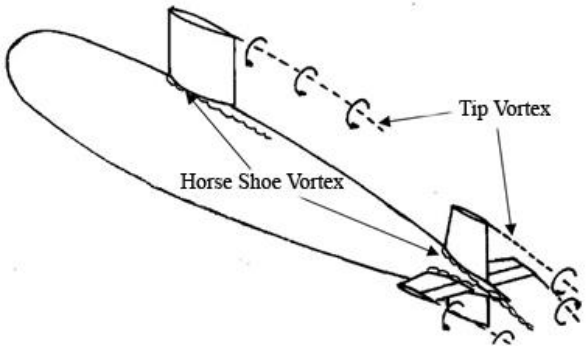

Fig. 1 Schematic of the formation of vortex structures on the submarine hull

junction of the sail and other appendages such as stern planes to the submarine hull.

Adding stern planes to the submarine hull will increase drag due to the creation of a pressure gradient, leading to an increase in the wet surfaces and spend some energy because of vortex production. The vortex moves downstream and enters the propeller flow at the end of stern, causing more turbulence in its flow. Therefore, the propeller inlet flow is accompanied by turbulence and vortex shocks. If the propeller operates in such a turbulent flow, the load on its blades is exerted in the peripheral direction. As a result, greater torque and propulsion force lead to a reduction in propeller efficiency due to reduced non-uniformity of inlet flow. In addition, the vibration and noise are increased in the propeller. The existence of noise produced by the submarine is not desirable. Thus, the propeller noise should be reduced as much as possible by using different methods. The noise produced by the propulsion system can be greatly reduced by using different equipment. A useful technique to improve the submarine's hydrodynamic performance is to control the flow of submarine peripheral components such as stern planes. The placement of these additional parts on the submarine hull leads to more complex flow field around it due to the addition of appendages' vortices. Therefore, in order to investigate the affective parameters, it is necessary to conduct the phenomenology of these vortex flows.

Investigation of the characteristics of flow around a submarine vehicle in the form of a line flow shaped body has been the focus of many researchers experimentally or numerically. Features such as the type and location of the boundary layer separation transition, the phenomenology of the various vortices formed around the hull and the additional parts of a submarine have been studied. Submarine model's wake flow has also been extensively studied by many researchers to evaluate the effects of turbulence and shear layers. Zhang *et al*. (2003) experimentally tested a submarine model with 5 different types of stern planes located at the stern area, in a towing tank and determined a stern plane with minimum non-uniformity. Jiménez *et al.* (2010) investigated the wake flow of the SUBOFF model with stern planes. Their results showed that the presence of the planes on the model causes great changes in off-wake velocity curves. It was found that the downstream area of the planes is associated with severe flow disturbances. The flow around a submarine model with a symmetrical hull and a sail was studied numerically and experimentally by Liu *et al.* (2011), (2010); Zhihua *et al*. (2011). They proposed an installation of a prismatic device in downstream to weaken the horseshoe vortex. After conducting numerical studies by installing the submarine model in a subsonic wind tunnel, they measured axial flow velocity in the stern area and compared numerical results with the experimental results. Posa and Balaras (2016) studied the SUBOFF model wake

flow with all its appendages numerically. They employed a structured grid with high grid resolution using LES turbulence model. Based on their results, the wake flow formed behind the sail is small and has no significant effect on the complexity of the passing flow field in the stern area and the wake flow of submarine at the impeller location. They concluded that the vortex resulting from the control surfaces' tips sheds much faster than the one resulting from the surface change in the stern area due to downward motion. They concluded that the complex vortex flow and adverse pressure gradient in the stern create a strong and complex vortex field at this area. Dubbioso *et al.* (2017) numerically studied the rotational capabilities of the submarine model with two X and cruciform shapes for control surfaces at the stern area with sail and other appendages. They created a multi-block mesh around the stern planes at the stern and other appendages such as sail and nose control surfaces. They concluded that the X arrangement for stern planes provides better rotation capability than the cruciform one. Rao and Yang (2017) simulated numerically a submarine's effective wake field using a combined approach and interpolation based on Radial Basis Function (RBF) method. Their method involved a combination of the panel method for the propeller using RANS equations for the hull and modeling the submarine self-propulsion motion. The method was able to predict the submarine wake flow accurately. Pan *et al.* (2019) solved the flow around SUBOFF G submarine model with appendages and propeller by using unsteady Reynolds averaged equations. They first investigated the submarine flow field without the impeller for different deflection angles of the stern planes under steady maneuver conditions. Then, they examined the flow on the submarine with the impeller. They carried out their investigations for straight ahead of the submarine and submerged maneuvers conditions. After examining the wake flow at the submarine end in term of non-uniformity at different angles of the stern planes, they asserted that the presence of hull appendages such as stern planes is the main source of producing non-uniformity and unsteady forces in the propeller. Fureby and Norrison (2019) studied the flow around a 6:1 prolate Spheroid at the incidence angles of $10°$ and $20°$ using RANS, Detached eddy simulation (DES), LES models. Their results showed that RANS and LES methods are of good capability in predicting the flow behavior in comparison with the experimental results. Carrica *et al*. (2019) investigated a general submarine model with a propeller near the surface in stationary and wavy waters numerically. In this study, they used the dynamic overset grid method around the hull, appendages and propeller to simulate the flow around the submarine. They compared the variations of the submarine flow field and the forces acting on it at different distances from the surface. Posa *et al.* (2019) investigated the wake flow of a submarine propeller using large eddy simulation method and compared their results with the experimental results obtained from velocity measurements test using *Particle image velocimetry* (PIV) method.

As stated earlier, the flow in the stern region is important due to several reasons. As the stern planes are located in the stern area, the flow in this region becomes more complex. The position of the control surfaces on the stern in different submarine designs has not been fixed and can be changed on the hull. By displacing the stern planes on the submarine hull, the size of the boundary layer encounters them will be changed. Hence, the position of the stern planes along the submarine's heel will affect its wake flow. Therefore, in this study, the optimum location for the stern planes is determined by moving them on the submarine to reduce the amount of non-uniformity and turbulence intensity of the propeller's inlet flow. In the next section, the governing equations of the present problem are presented.

2. Governing equations

In this section, the governing equations used to simulate the flow around the submarine model are described. The governing hydrodynamic equations for the fluid flow are continuity and momentum equations. These differential equations are obtained using Newton's second law on small fluid volume control in the laminar flow. They are converted into solvable equations on the computational grids using finite volume method. In this study, the Reynolds averaged Navier-Stokes method is used for modeling the turbulent flow. In fact, the purpose of these equations is to determine the velocity at a given position in time series. In this method, the velocity is divided into two components: mean velocity $\overline{U}$ and turbulent component u. These two components are added to the equations in the laminar form of Navier-Stokes equations. An averaging and simplification of the Navier-stokes equations for turbulent flows are as follows

$$U = u + \overline{U} \tag{1}$$

$$\frac{\partial \overline{U}_i}{\partial t} + \overline{U}_j \frac{\partial \overline{U}_i}{\partial x_j} = \frac{1}{\rho} \frac{\partial}{\partial x_j} \left(-p\delta_{ij} - \rho \overline{u_i u_j} \right) \tag{2}$$

In these equations p is the pressure, $\overline{U}$ the mean velocity, u the transient component and δ_{ij} the *Kronecker* delta.

The second term of right-hand side of Navier-Stokes equations related to the Reynolds stress tensor that is estimated using Boussinesq equation

$$-\rho \overline{u_i u_j} = \rho \nu_t \left(\frac{\partial v_i}{\partial x_j} + \frac{\partial u_j}{\partial x_i} \right) - \frac{2}{3} \rho k \delta_{ij} \tag{3}$$

where ν_t is the turbulent viscosity. By substituting the Boussinesq equation into the above equation

$$\frac{\partial U_i}{\partial t} + U_j \frac{\partial U_i}{\partial x_j} = \frac{1}{\rho} \frac{\partial}{\partial x_j} \left(-p\delta_{ij} + \left(\rho \nu_t \left(\frac{\partial v_i}{\partial x_j} + \frac{\partial u_j}{\partial x_i} \right) - \frac{2}{3} \rho k \delta_{ij} \right) \right) \tag{4}$$

Here the relationship between the turbulent viscosity and turbulence diffusion coefficient is

$$\nu_t = \sigma_t \Gamma \tag{5}$$

where Γ is the diffusion coefficient and σ_t is the Schmidt number.

The turbulence models are divided according to the number of equations to relate the turbulence pressures to the averaged velocity or its gradient. Here, because of the capabilities of $k-\varepsilon$ turbulence model in the prediction of high inverse-pressure-gradient flows, this model is used. The computational cost of this model is low. It also has good accuracy, focusing on functions that affect turbulent kinetic energy. The standard $k-\varepsilon$ model has two additional equations, one for k and the other for ε to better understand the processes that cause these variables to change. This two-equation model describes the turbulent viscosity as follows

$$\nu_t = c_\mu \frac{k^2}{\varepsilon} \tag{6}$$

The turbulent viscosity is expressed in terms of the rate of turbulence generation and dissipation, where k is obtained from this relation

$$k^2 = \frac{1}{2}\left(\overline{u_i u_j}\right) \tag{7}$$

The part of the k equations in the tensor form is modeled as follows

$$\frac{\partial k}{\partial t} + U_i \frac{\partial k}{\partial x_i} = \frac{\partial}{\partial x_i}\left(\frac{\nu_t}{\sigma_k}\frac{\partial k}{\partial x_i}\right) + p_k - \varepsilon \tag{8}$$

$$p_k = \nu_t \left[\frac{\partial u_i}{\partial x_j} + \frac{\partial u_j}{\partial x_i}\right]\frac{\partial u_i}{\partial x_j} \tag{9}$$

In this equation, k is the generation of turbulence, ε is its depreciation, U_i is the average velocity, and υ_t is the turbulent viscosity. And, the dissipation rate ε is expressed by the following equation in the tensor form

$$\frac{\partial \varepsilon}{\partial t} + u_i \frac{\partial \varepsilon}{\partial x_i} = \frac{\partial}{\partial x_i}\left(\frac{\nu_t}{\sigma_\varepsilon}\frac{\partial \varepsilon}{\partial x_i}\right) + c_1 \frac{\varepsilon}{k} p_k + c_2\left(\frac{\varepsilon^2}{k}\right) \tag{10}$$

In this study, the dimensionless turbulence intensity parameter is used to determine the amount of fluid flow turbulence

$$T.I = \frac{\sqrt{\frac{2}{3}k}}{U_{mean}} \tag{11}$$

3. Definition of the problem

The purpose of this study is to investigate the effect of the location of the stern planes on improvement of wake flow at the propeller position of a submarine model. Numerical simulations are performed for the flow around a SUBOFF submarine model with a total length of 70 cm in a laboratory scale with cruciform for stern planes under fully submerged condition. A schematic of the submarine model is shown in Fig. 2. In order to investigate the effect of changing the position of the stern planes, the measurements are carried for three locations of fins' end relative to the nose of the model at the stern area (Fig. 3). In addition to the no-deflection angle stern planes, measurements are also performed for the case in which the stern planes have deflection angles of $\delta = 5°, 10°, 15°$ to study the wake flow of submarine at initially states of maneuvering movements. Finally, the results are compared for three stern planes positions to find a better location in terms of the lowest non-uniformity and turbulence of the wake flow at the propeller location. To do this, the average velocity and the axial wake flow turbulence at the propeller location, as well as the coefficients of pressure and drag on the hull, are presented for three locations of the stern planes.

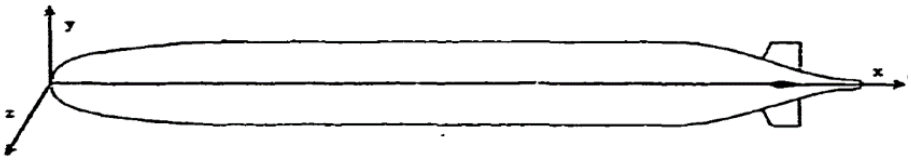

Fig. 2 Schematic of the DARPA SUBOFF submarine model with coordinate system

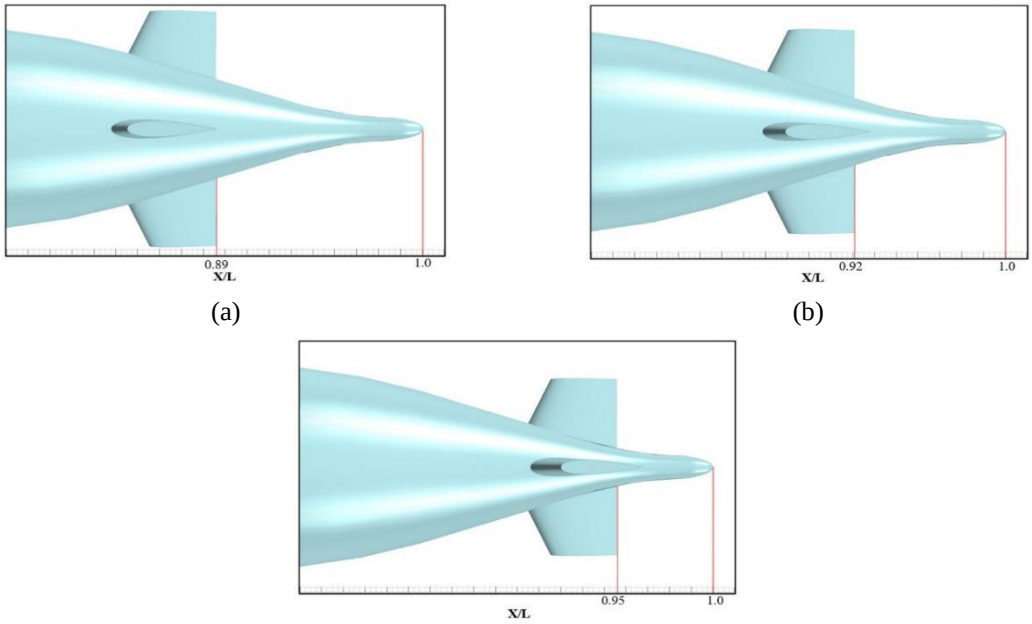

Fig. 3 Schematic of the location of the control surfaces on the stern of submarine while their position from the nose is: (a) X/L=0.89, (b) X/L=0.92, (c) X/L=0.95

3.2 Computational domain and boundary conditions

In order to simulate the flow around the submarine model, the model geometry is generated according to the Table 1. Then, to solve the flow around the stern planes more precisely as well as to prevent from an incremental increase in the number of computational grid elements, and also to change the grid formed around the model, a multi-block overset grid method is used around the submarine model stern planes. For the SUBOFF model, the standard cruciform for the stern planes with NACA0020 cross-sectional area and $25°$ sweep angle is proposed by the manufacturer Groves *et al.* (1989).

In order to solve the flow field around the submarine model, appropriate boundary conditions must be defined. Since the present study aims to examine the fluid flow structure around the submarine under full submerged conditions, the boundary conditions are considered as the flow around the submarine model does not affected by buoyancy and free surface. The computational

domain in the present study consists of a submarine model hull with the stern planes embedded in a rectangular space. In order to achieve more realistic results, the submarine model should be sufficiently distant from the walls. No-slip boundary condition is used for the model surface and upper and lower walls. Velocity-inlet and pressure-outlet are used for inlet and outlet sections, respectively. The geometry, computational grid and numerical simulations are performed using the commercial software of STAR CCM+. Fig. 4 shows the computational domain along with the submarine model and boundary conditions.

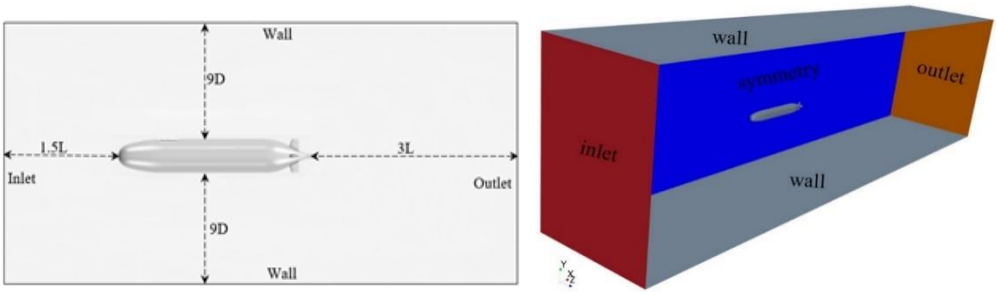

Fig. 4 Computational domain with boundary conditions in the present study

Table 1 Geometric properties of the SUBOFF model

Model's total length	$0.7m$
Model's total diameter	$0.08m$
Control surface's side cross-sectional area	$0.298m^2$
Control surface's dimension ratio	0.72
Control surface's cross section profiles	NACA0020

4. Numerical validation and mesh study

As mentioned in the previous sections, depending on the subject of the study, it is necessary to move some parts of the submarine model geometry into the flow field. Because of the advantage of multi-block overset grid in meshing the complex geometries with several separate parts, in this research, the overset grid method is used to avoid the mesh change created on different parts of the submarine. In the overset grid method, a separate grid is constructed around each part of the studied object so that this grid can move and rotate easily within each other. Also, some parts of the grid can be positioned outside the solution area. The mesh created in this study consists of a main grid on the bare hull of the submarine model across the flow field and four sub-grids created on the stern planes as overset grids (Fig. 6). The distribution of the mesh elements is such that the thickness of the first layer is maintained at a range of $y^+ = 30-60$, which is suitable for the wall function. This grid is assumed to be constant in the present study. The simulations are performed by moving sub-grids within the main one and moving the stern plane onto the main hull. In order to investigate the grid independency of the numerical simulations, the values of moment and drag coefficients are

calculated on the hull for four grids with different numbers of elements, in accordance with Table 2. Fig. 5 shows the difference between the predicted values obtained from different computational grid compared to the finest one. As can be seen in this figure, two grid resolutions of 3 and 4 predict the quantities slightly different. In addition, since the reduction in the computational cost is very important, therefore, grid 3 is chosen. Fig. 6 shows an overview of the grid created on the submarine model with stern planes with the deflection angle of $\delta = 5°$.

The present study aims at investigate the effect of the longitudinal position of stern planes located on the submarine stern on the surrounding flow field as well as the wake flow formed at the rear of the submarine. Unfavorable pressure gradients and flow separation from the surface have complexities, leading to that the prediction of the flow behavior in this area inaccurate. Therefore, in the following sections, the flow field is evaluated in terms of different values of pressure, friction, the moment applied to the hull, flow velocity and turbulence intensity by moving the control surfaces on the submarine's stern.

In order to validate the numerical simulation method, the fluid flow around the submarine model is simulated when the stern planes are not mounted on the submarine hull. So, the distribution of dimensionless friction coefficient (Fig. 7(a)) and pressure coefficient (Fig. 7(b)) over the hull are compared with the experimental results measured by Huang *et al*. (1994). As can be seen in these figures, there is no difference between the predicted coefficients of the present study and those of experimental results. Then, after verification of the results, the coefficients of friction and pressure are compared by placing control surfaces at three longitudinal positions.

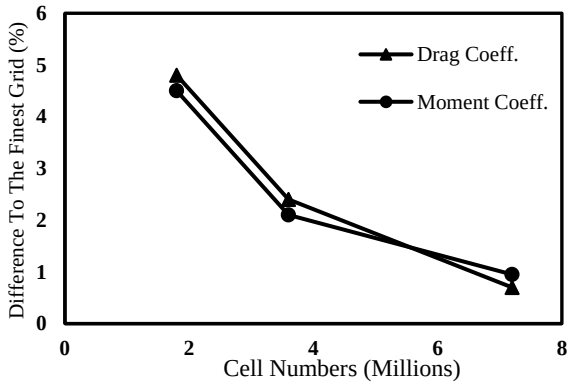

Fig. 5 The grid study of numerical simulations in the present work

Table 2 The number of elements in the four grids used

	Grid **1**	Grid **2**	Grid **3**	Grid 4
Control Surfaces	820000	1650000	3240000	6430000
Hull	1055000	2130000	415000	83200000
Total	1875000	3780000	7390000	14750000

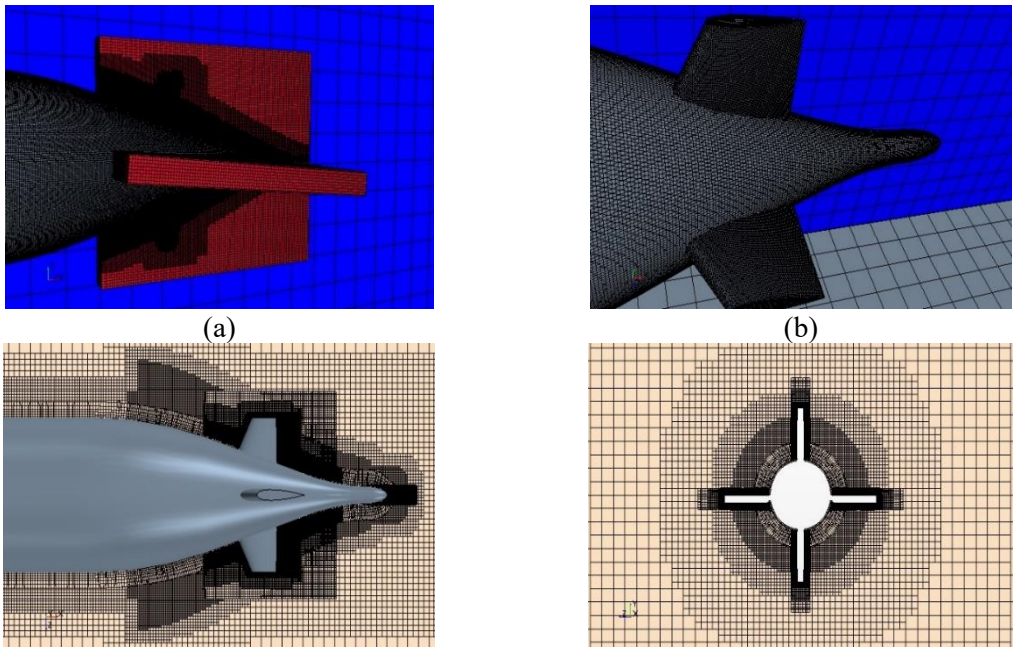

Fig. 6 Grid created on the submarine model with stern planes:(a) Grid created along with overset block grids around the stern planes, (b) Grid created on the model after hole-cutting of the overset areas (C) Grid created on in the middle plane of the model (d) Grid created on the model at a distance of $X/L = 0.9$, in the y-z plane

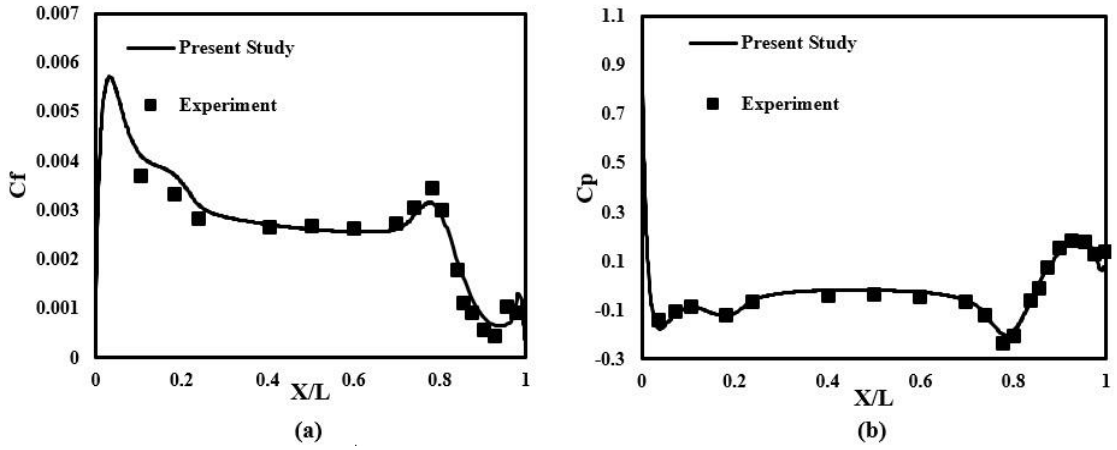

Fig. 7 Comparison between the non-dimensional friction and pressure coefficient on the hull of submarine without stern planes (Bare Hull) and experimental results of Huang *et al.* (1994): (a) friction coefficient and (b) pressure coefficient

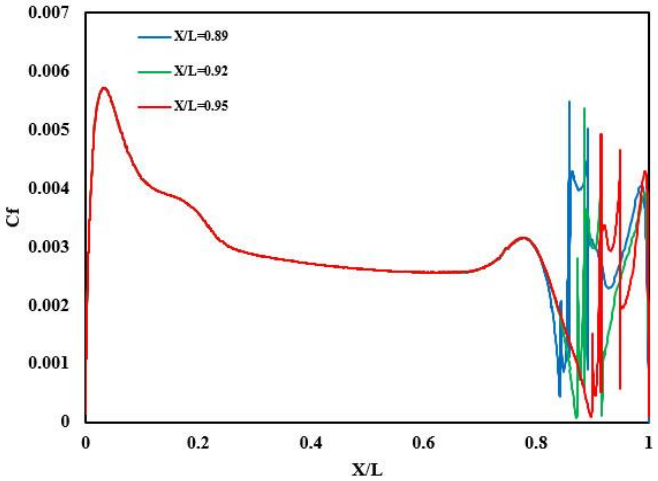

Fig. 8 Comparison of friction coefficient on the hull when stern planes are installed at $X/L=0.89$, $X/L=0.92$, $X/L=0.95$

5. Comparison of friction and pressure coefficients on the submarine hull

Fig. 8 shows the distribution of the surface friction coefficient on the submarine hull for four states with/without stern planes at longitudinal distances of $X/L=0.89,0.92,0.95$. It can be seen that the friction coefficient value when the stern planes are mounted at $X/L=0.95$ is generally lower than the other two cases. For two distances of $X/L=0.92,0.95$, although the values of friction coefficient at the beginning and end of the stern planes at distance $X/L=0.92$ are greater than $X/L=0.95$, the overall value of the friction coefficient behind the stern planes for the longitudinal distance $X/L=0.95$ is greater than $X/L=0.92$. This implies that the amount of turbulence within the boundary layer for the stern planes installation at $X/L=0.92$ is lower than the other ones because the friction coefficient on the hull indicates the shear stress within the boundary layer close to the surface. So, the shear stress value within the boundary layer also depends on the turbulence value inside the boundary layer.

In Fig. 9, the distribution of pressure coefficient on the submarine model hull is plotted for the four states with/without the stern planes at $X/L=0.89,0.92,0.95$, respectively. This figure shows that the pressure coefficient is increased immediately at the leading edge of the stern planes by mounting the stern planes on the stern area. After that, it decreases immediately and then increases gradually again once the flow is completely separated from the submarine hull. The pressure value is generally greater when the stern planes are mounted at a distance of $X/L=0.89$ than the other cases. For the case in which the stern planes are mounted at a distance of $X/L=0.95$, this value is approximately less than the other ones, leading to an increase in the stability of the stern planes in this area. It can also be said that the pressure gradient for this state is lower than the other ones, resulting in a

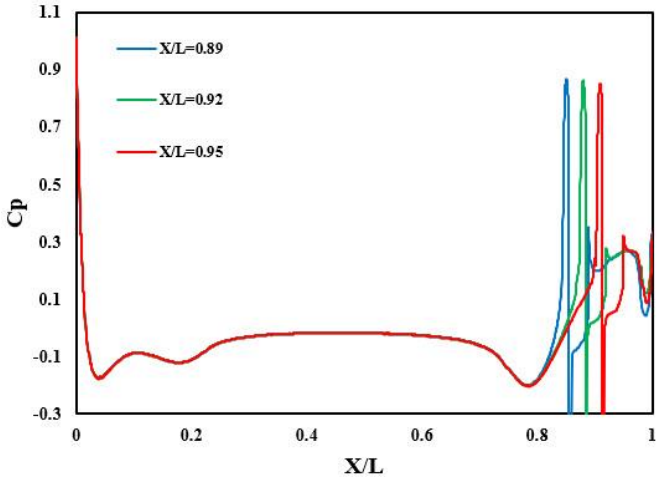

Fig. 9 Comparison of pressure coefficient on the hull when stern planes are installed at $X/L=0.89$, $X/L=0.92$, $X/L=0.95$

reduction in the cavitation phenomenon in this region. Finally, at this section it can be concluded that the installation of stern planes at a distance $X/L=0.89$ is not desirable from the points of view of pressure and friction distribution. As well, for the case of stern planes at distances $X/L=0.92$ and $X/L=0.95$, it can be said that although they are not too different from one another in terms of pressure and friction distribution, the installation of the stern planes at $X/L=0.95$ provides better conditions duo to their stability and the cavitation possibility reduction.

6. Flow field around the hull along with stern planes

6.1 Drag force and moment on the hull

The positioning of the stern planes exerts more frictional force on the submarine hull, and any change in their location may also change the size of the friction force. Fig. 10 compares the amount of friction coefficient on the submarine model hull for the stern planes with the deflection angle of ($\delta = 0°, 5°, 10°, 15°$) and three longitudinal distances of $X/L=0.89, 0.92, 0.95$. As the figure shows, the friction value for all states increases with the deflection angle of the stern planes. The friction rate also increases with the distance from $X/L=0.95$ to $X/L=0.89$. The friction coefficient difference is also greater when the stern planes protruded out of the hull width ($X/L=0.89$) and this difference is further increased by increasing the deflection angle of the stern planes. Therefore, it can be said that the installation of stern planes at a distance of $X/L=0.95$ will reduce the overall frictional force applied by the fluid to the submarine.

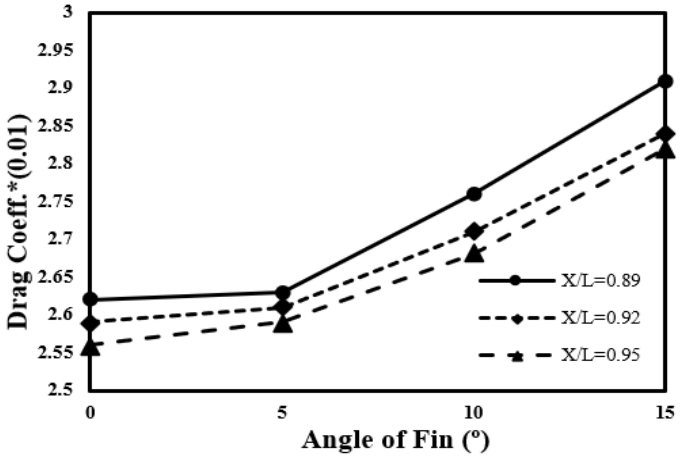

Fig. 10 Comparison of drag coefficient on the hull for three locations of the control surfaces on the stern at the angles of $\delta = 0°, 5°, 10°, 15°$

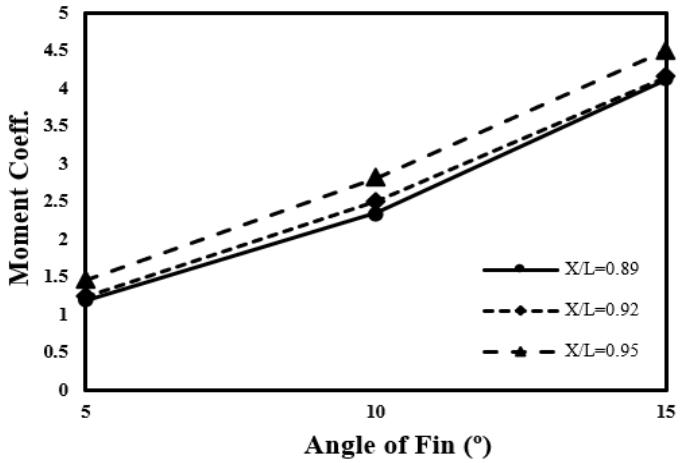

Fig. 11 Comparison of the moment coefficient applied to the hull around the center of mass for three locations of the control surfaces on the stern at the angles of es $\delta = 5°, 10°, 15°$

The main purpose of mounting the stern planes on the submarine hull is to apply the moment around its mass center to change the direction of the submarine and drives it in the specified direction. So, it is natural that any change in the appearance or location of the planes should result in their better performance. In this section, the amount of moment coefficient applied by the stern planes to the submarine model is calculated. In Fig. 11, the coefficient of moment applied to the hull by the stern planes on the y-x plane around the submarine's model center of mass at the longitudinal position $X/L = 0.4621$ is plotted for horizontal stern planes with three locations of $X/L = 0.89, 0.92, 0.95$ and different deflection angles of $\delta = 0°, 5°, 10°, 15°$. Since, at fully submerged conditions when the stern planes are mounted on the hull, there is no difference between

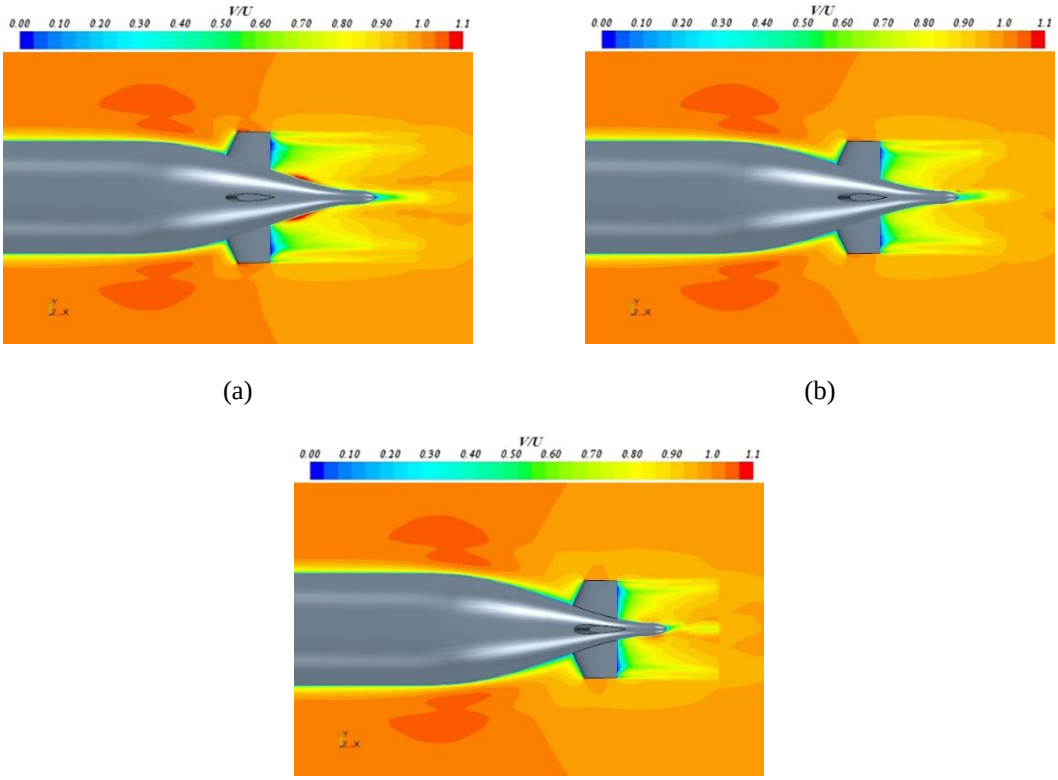

Fig. 12 Comparison of the distribution of flow average velocity on the x-y plane at the submarine model end for the three locations of the stern planes without deflection angle: (a) $X/L=0.89$, (b) $X/L=0.92$, (c) $X/L=0.95$

the stern planes on the horizontal and the vertical planes. Thus, the deformation of the horizontal stern planes is considered as sufficient. As this figure shows, the amount of moment applied to the hull increases almost linearly by increasing the deflection angle. In addition, the installation of stern planes at distances $X/L=0.89,0.92$ does not significantly alter the amount of moment applied to the hull. However, the installation of stern planes near the end of the heel ($X/L=0.95$) causes an effective increase in the moment applied to the hull. Therefore, it can be concluded that whether in terms of frictional force applied to the hull or in term of better controllability, the installation of stern planes at the longitudinal position of $X/L=0.95$ is be more effective.

*6.2 Stern planes with $\delta=0°$ *

It is generally expected that placing stern planes on the hull results in the flow field around the submarine becomes more complicated. The displacement of these surfaces on the stern causes some changes in the flow field around the submarine and in the stern area. So, wake flow will be also

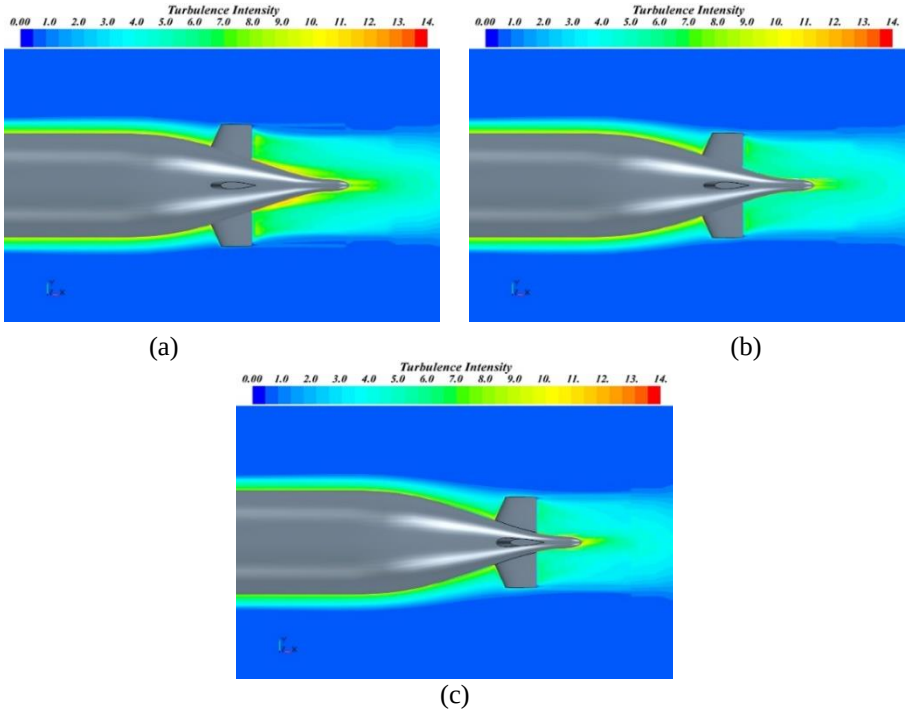

Fig. 13 Comparison of the turbulence intensity on the x-y plane at the submarine model end for the three locations of the stern planes without deflection angle: (a) $X/L=0.89$, (b) $X/L=0.92$, (c) $X/L=0.95$

changed at the stern end. In this section, the flow behavior in the stern area is studied for different positions of stern planes by presenting velocity contours, turbulence intensity contours, and streamlines. Fig. 12 shows the average flow velocity contour on the submarine model while the stern planes are mounted at three locations of $X/L=0.89,0.92,0.95$. It is observed that the main characteristic of the flow around the submarine model along with the stern planes is the wake and vortex flows near their tip and the flow near the hull. It should be noted that these features have been mentioned in many previous numerical studies. According to this figure, when the stern planes are at a distance of $X/L=0.89$, a high average velocity flow field is formed behind the stern planes (near the stern surface) due to the interference of the flow with the boundary layer on the stern surface. For the case of stern planes at the position of $X/L=0.92$, no increase is observed near the stern surface. When the stern planes were located at $X/L=0.95$, there is some increase in the average velocity near the stern surface. Although this difference is not as large as the velocity difference for the case in which the stern planes is at $X/L=0.95$, the average flow rate at the stern end and the propeller position increase. Another issue that can be pointed out in this figure is that although the transfer of control surfaces to the stern end results in an extension of the wake region along the flow and along the submarine model hull, it causes that the space influenced by the stern planes wake flow in the stern area to reduce greatly compared to the other modes (i.e., $X/L=0.89,0.92$).

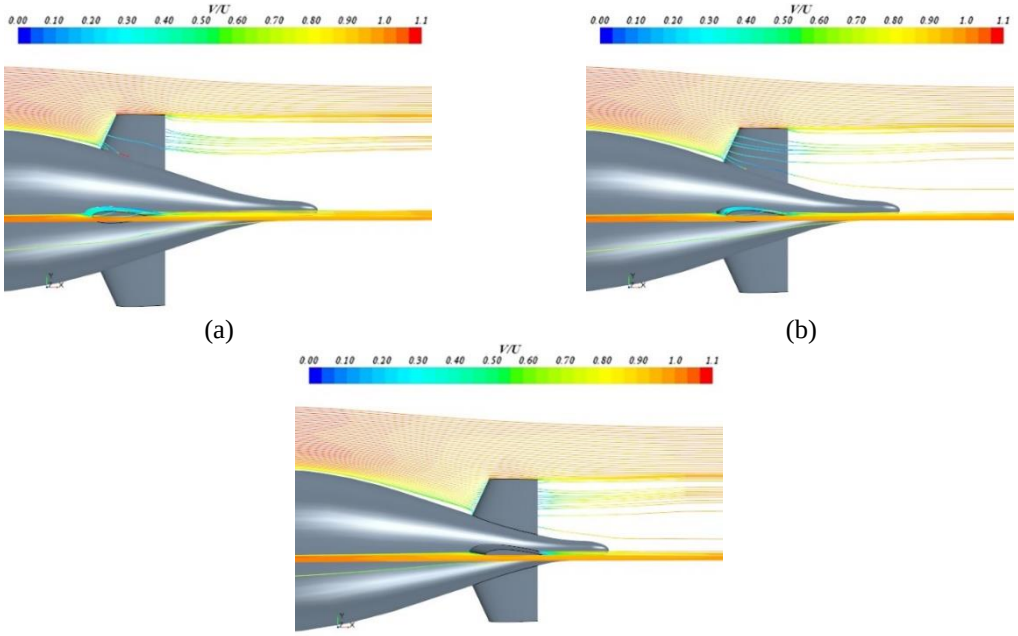

Fig. 14 Comparison of the streamlines on the x-y plane at the submarine model end for the three locations of the stern planes without deflection angle: (a) $X/L=0.89$, (b) $X/L=0.92$, (c)

In Fig. 13, the turbulence intensity contour of the flow around the submarine model is plotted for three locations of the stern planes (i.e., $X/L=0.89,0.92,0.95$). As can be seen for all three shapes, there is almost no difference in the turbulence intensity on the hull before the stern planes, and the flow behavior around the stern plane is such that the amount of turbulence intensity produced on the submarine stern decreases by moving the surfaces from the model nose ($X/L=0.89$) to the stern ($X/L=0.95$). By decreasing the turbulence intensity, it is expected the surface friction coefficient decreases due to the reduction of shear stress in the near-hull layer. Therefore, in terms of the amount of turbulence intensity on the hull and stern, it can be concluded that it is more appropriate to install stern planes at the distance of $X/L=0.95$, when the submarine device is not in maneuvering condition, i.e. the stern planes have no deflection angle ($\delta=0°$).

In Fig. 14, the streamlines are plotted on the submarine model hull and in the stern area while the stern planes are mounted at three locations of $X/L=0.89,0.92,0.95$. As can be seen in this figure, the streamlines behave nearly the same before reaching the stern planes. However, they behave differently when they collide with the control surfaces in the stern area. As for the case in which the control surfaces are at the location of $X/L=0.89$, streamlines tend to move from the stern surface to the control surfaces tip. However, the tendency is reduced as these surfaces move away from the nose and approach the end of the stern. Hence, when the stern planes are in the longitudinal position of $X/L=0.95$, the streamlines in the stern area and on the control surfaces will be more evenly distributed. More uniform streamlines on the control surfaces leads to an increase in their efficiency, resulting in a uniform flow into the propulsion system and improvement of its performance.

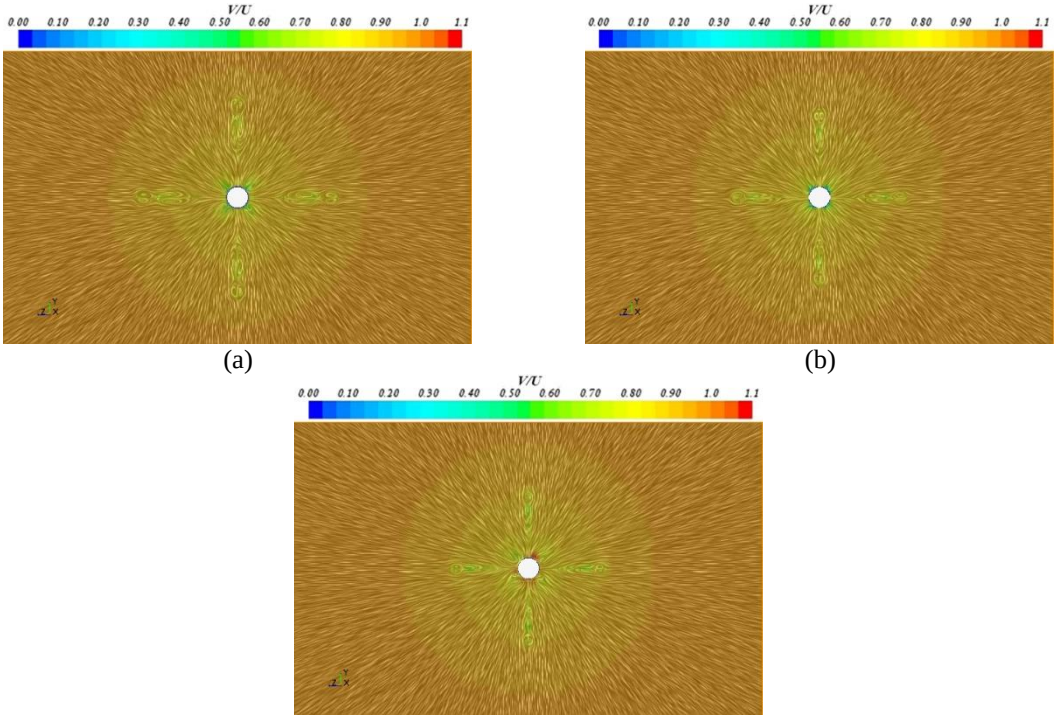

Fig. 15 Comparison of the flow pattern on the y-z plane at the position of propeller (X/L=0.978), for the three locations of the stern planes without deflection angle: (a) $X/L=0.89$, (b) $X/L=0.92$, (c) $X/L=0.95$.

After passing through the submarine hull, the fluid flow is separated as a wake flow that is expanded along its length. The submarine propeller is the first and foremost part which the hull wake flow enters into it and requires the least amount of non-uniform flow to have better performance in terms of generating the propulsion force with the least noise and turbulence. In this section, the vectors, velocity contours and turbulence intensity contours are presented to compare the wake flow formed at the submarine end due to the stern planes.

In Fig. 15, the integrated velocity vectors are plotted on the y-z plane at the distance of $X/L=0.978$ from the nose, where the submarine propeller is installed at three longitudinal distances of $X/L=0.89,0.92,0.95$. As can been seen in these figures, due to the effect of each stern plane on the submarine heel, two pairs of specified vortices are created in the wake area. The location of the submarine propeller shows that each of which consists of two vortices with opposite rotational directions. One of them consists of stern planes wake and other one consists of stern planes tip vortex. For the case the stern planes mounted at the distance of $X/L=0.89$, it is observed that the width of each vortex and tip vortex pair is greater than that in the other cases, such that width of the two vortices and tip vortex pair are the lowest for the case where the stern planes distance from the nose is $X/L=0.95$. In addition, since the vectors have been colored with velocity

characteristics, it can be seen that in this case, the average velocity value in the propeller location is higher than that in the other ones.

In Fig. 16, the average velocity contour on the y-z plane at the longitudinal distance of $X/L=0.978$ from the nose is plotted for the longitudinal distances of the stern planes of $X/L=0.89,0.92,0.95$ where the wake flow enters the propulsion system. It is demonstrated that by moving from $X/L=0.89$ to $X/L=0.95$, the average velocity at the position of the stern planes wake flow and the tip vortices decrease. As shown in Fig. 12, by moving from the nose to the end of the stern, the amount of wake elongation at the stern position decreases, resulting in a decrease in the average velocity of the stern planes' wake due to the decrease in their influence domain. Moreover, the reduction rate of the average velocity resulting from the stern planes approach to the propeller plane is lower than that was expected. As shown in this figure, there is a decrease in the velocity between the stern planes wake flow that are horizontally located and the stern planes located on the vertical plane, caused by the interference of the boundary layer flow on the stern surface and the flow induced by the stern planes. Thus, when the stern planes are at the distance of $X/L=0.95$, the interference level is reduced and the average velocity is increased in this position. When the stern planes are at the distance of $X/L=0.95$, one can observe the minimum wake width of the hull, as well as the stern planes wake and tip vortex flows relative to the other cases. It can be concluded that when the submarine device is in non-maneuverable condition and the stern planes have an angle of $\delta=0°$, an increase occurs in the average velocity near the surface and operating area of the propeller with a slight decrease in the average velocity at the position of the stern planes wake flow. This is done by placing the control surfaces at a longitudinal distance $X/L=0.95$ towards the end of the stern.

Fig. 17 shows the turbulence intensity contour for the longitudinal distances of the stern planes, i.e. $X/L=0.89,0.92,0.95$ from the nose at the y-z plane and at the longitudinal distance $X/L=0.978$ from the nose, where the submarine propeller is located. It can be concluded that for the case where the stern planes are at the distance of $X/L=0.95$, the minimum turbulence intensity width is observed in the whole wake flow. Also, the magnitude of the increase in the turbulence intensity resulting from the wake flow and the tip vortices at the stern planes at a distance of $X/L=0.95$ is lower than that obtained from the other cases. In addition, the value of the turbulence intensity near the surface and operating area of the propeller is approximately less than that of the other distances for the distance of $X/L=0.95$. It can be concluded that when the stern planes have no deflection angle, their installation at $X/L=0.95$ generally provides better conditions.

In Fig. 18, the dimensionless average velocity is presented on the y-z plane at the longitudinal distance of $X/L=1$ and $Y/R=0$ for three positions of the control surfaces at $X/L=0.89,0.92,0.95$. As this figure shows, in all three cases, the velocity curve that moves in the transverse direction from the center of the model to the outside has a decrease at these points. These points represent, respectively, the hull wake interfering with the flow attached to the stern surface belonging to the control surfaces, the wake flow formed behind the control surfaces, and the vortex flow at the tip of the control surface. The highest average velocity decreases in the middle part related to the wake flow of the control surfaces. Finally, the minimum average velocity decrease is at the edges of the control surfaces. After that, the average flow velocity diagram reaches a constant value indicating the free stream. As the control surfaces move from $X/L=0.89$ to $X/L=0.95$, their transverse position also moves closer to the center of the model. Thus, one can expect that their

wake flow moves toward the center of the model and this is clearly visible in Fig. 18. Faster wake flow segment tends to move toward the free stream, the wake width becomes smaller, which is evident for the distance of $X/L=0.95$. In other words, the wake width in this case is reduced compared to the hull width of two distances of $X/L=0.89, 0.92$. However, since the main purpose of improving a submarine flow is to improve the inlet flow to the propeller, the flow is in focus at a distance less than the impeller radius, i.e. $Z/R \le 0.5$. The remarkable point in this figure is that, as the stern planes move away from the nose ($X/L=0.89$) and move towards the stern end ($X/L=0.95$), the average velocity in the center of the submarine model wake flow is increased. As well, the non-uniformity of the wake flow decreases. As seen in this figure, at a radius lower than the radius of the submarine propeller ($Z/R=0.5$), when the stern planes are mounted at a distance of $X/L=0.89$, the ratio of the minimum velocity at line Y=0 to the velocity of freestream is $u_{min}/U=0.48$, while this ratio is increased to $u_{min}/U=0.85$ for the case in which the stern planes are mounted at a distance of $X/L=0.95$.

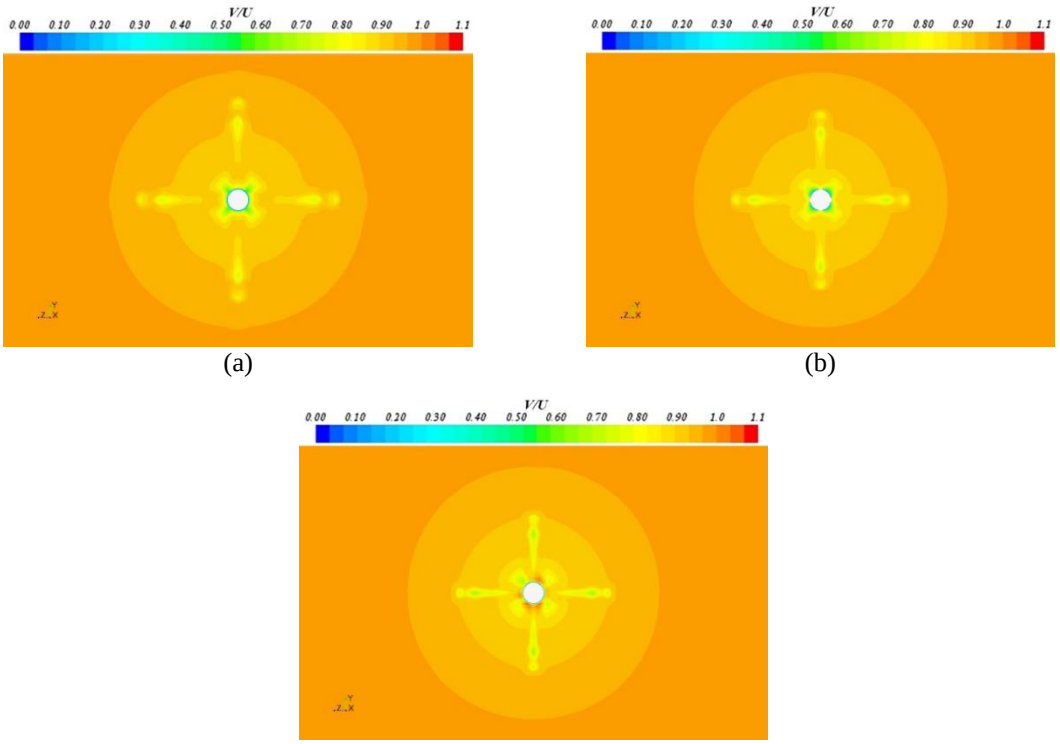

(a) (b)

(c)

Fig. 16 Comparison of the distribution of flow average velocity on the location of the submarine propeller (on the y-z plane at the cross-section $X/L=0.978$) for the three locations of the stern planes without deflection angle: (a) $X/L=0.89$, (b) $X/L=0.92$, (c) $X/L=0.95$

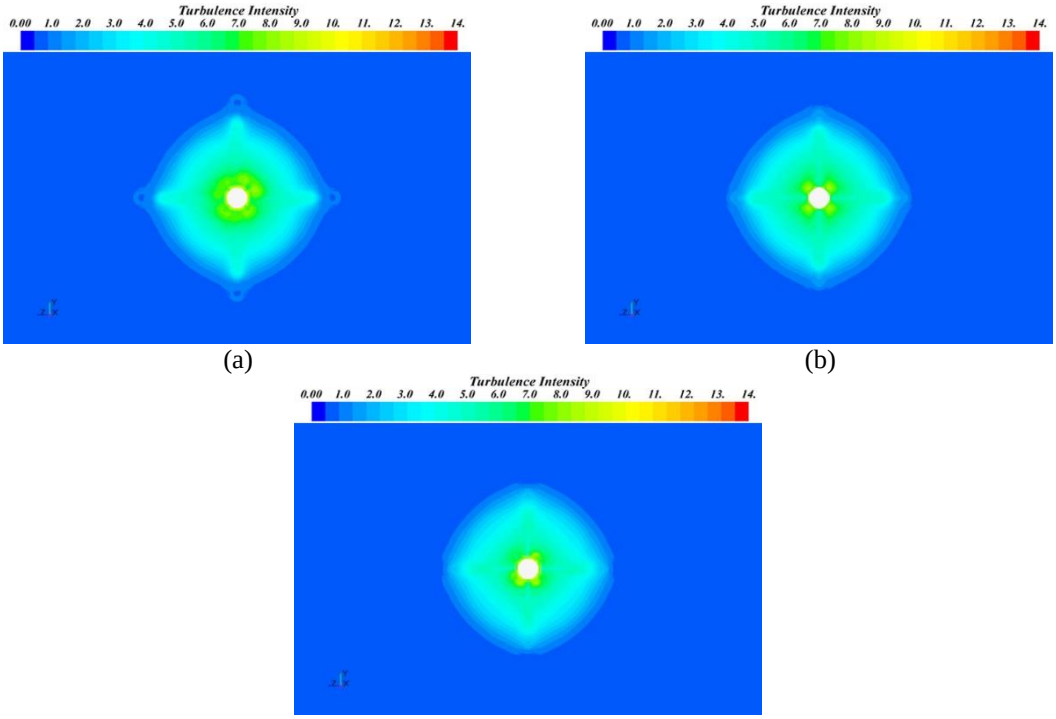

Fig. 17 Comparison of the turbulence intensity on the location of the submarine propeller (on the y-z plane at the cross-section $X/L=0.978$) for three locations of the stern planes without deflection angle: (a) $X/L=0.89$, (b) $X/L=0.92$, (c) $X/L=0.95$

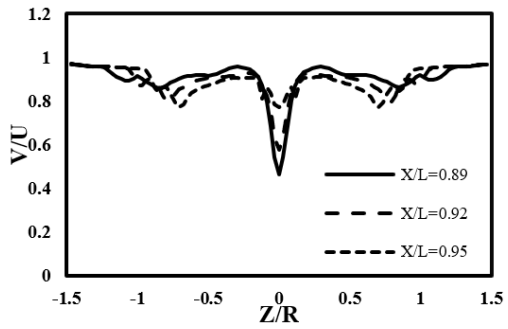

Fig. 18 Average velocity diagram in transverse direction at $Y/R=0$ from center of submarine model for three locations of stern planes

Therefore, it can be concluded that, generally, more uniform flow can be provided to the propeller by installing stern planes at a distance of $X/L=0.95$ from the nose. The average velocity diagram for $X/L=0.95$ also shows a decrease in the velocity due to the entry of junction flow or the horseshoe vortex belonged to the stern planes. It has not much effect on the non-uniformity of the inlet flow to the propeller.

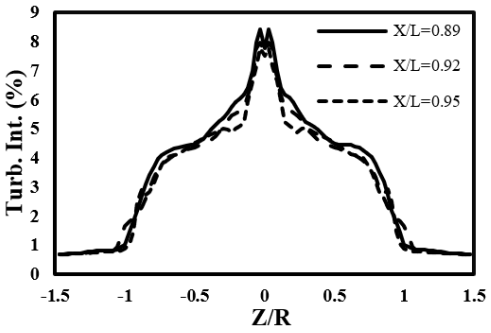

Fig. 19 Turbulence intensity diagram in transverse direction at $Y/R=0$ from center of submarine model for three locations of stern planes

In Fig. 19, the turbulence intensity diagram is presented on the y-z plane at the longitudinal distance of $X/L=1$ from the model nose as well as at $Y/R=0$ from the model center along the z-axis for three stern planes at $X/L=0.89,0.92,0.95$. As seen in this figure, for the case where the stern planes of the submarine model have no deflection angle, the turbulence intensity diagram belonging to the state at which the surfaces are at $X/L=0.89$, is greater than that of the other two cases in terms of the maximum magnitude and the width value. For the case where the stern planes are mounted at the distance of $X/L=0.95$, the diagram is smaller in magnitude and width compared to other cases.

6.3 stern planes with deflection angle

The submarine device commonly needs to change its direction by changing the angle of the control surfaces at the heel. In this case, the wake flow formed at the stern is entered to the propeller, so it is necessary to investigate the wake flow in the maneuver conditions.

In Fig. 20, the velocity vectors on the y-z plane at a distance of $X/L=0.978$ from the nose (i.e. the location of the submarine propeller) are plotted for three installation locations of the stern planes $X/L=0.89,0.92,0.95$. This is while the surfaces located on the horizontal plane z-x have a deflection angle of $\delta=5°$ around the z-axis. As can be seen in these figures, the wake flow formed behind the submarine model undergoes widespread changes to those surfaces without any angles by rotating the stern planes, leading to a complexity of the wake due to the hull flow in the stern area. Therefore, the prediction of the flow behavior in different situations becomes impossible. The stern planes with a deflection angle of $\delta=5°$ cause the wake flow of the submarine model to change. Behind the horizontal stern planes, instead of the previous two weak vortex pairs, a single vortex with much greater width and power is generated in the wake for all three longitudinal positions. The amount of vortex occupied by the vortex produced by the stern planes is the highest at $X/L=0.89$ and is the least at the distance $X/L=0.95$ among all cases. The vortex flows created by the horizontal stern planes also cause changes in the vortex flows formed at the bottom of the vertical stern planes. Two pairs of the upper vortices become much weaker and the two pairs of the lower vortices exhibit greater elongation. However, this elongation is the maximum value for the stern planes mounted at $X/L=0.89$ and the lowest value for the stern planes corresponds to

$X/L=0.95$. For the center section, there also seems to be a tendency for a pair of symmetrical vortices to form at the bottom of the surface, that the tendency for stern planes at $X/L=0.89$ is greater than the other cases.

In Fig. 21, the average velocity contour on the y-z plane at a distance of $X/L=0.978$ from the nose is plotted for three locations of the stern planes, $X/L=0.89, 0.92, 0.95$. The surfaces located on the horizontal plane x-z has have a deflection angle ($\delta=5°$) around the z-axis. It can be concluded that the average velocity decreases somewhat at the wake flow position of the stern planes as well as the tip vortices by moving from $X/L=0.89$ to $X/L=0.95$. Also, the decrease in the velocity due to the interference of the boundary layer flow on the stern surface and the flow resulting from the control surfaces between the horizontal and vertical stern planes is lower for the case of the stern planes at a distance of $X/L=0.95$ than other two cases. Also, the average velocity is higher. While the stern planes are at the distance of $X/L=0.95$, the overall width of the hull wake flow, the stern planes wake flow and their tip vortex flow is less than that of the other cases.

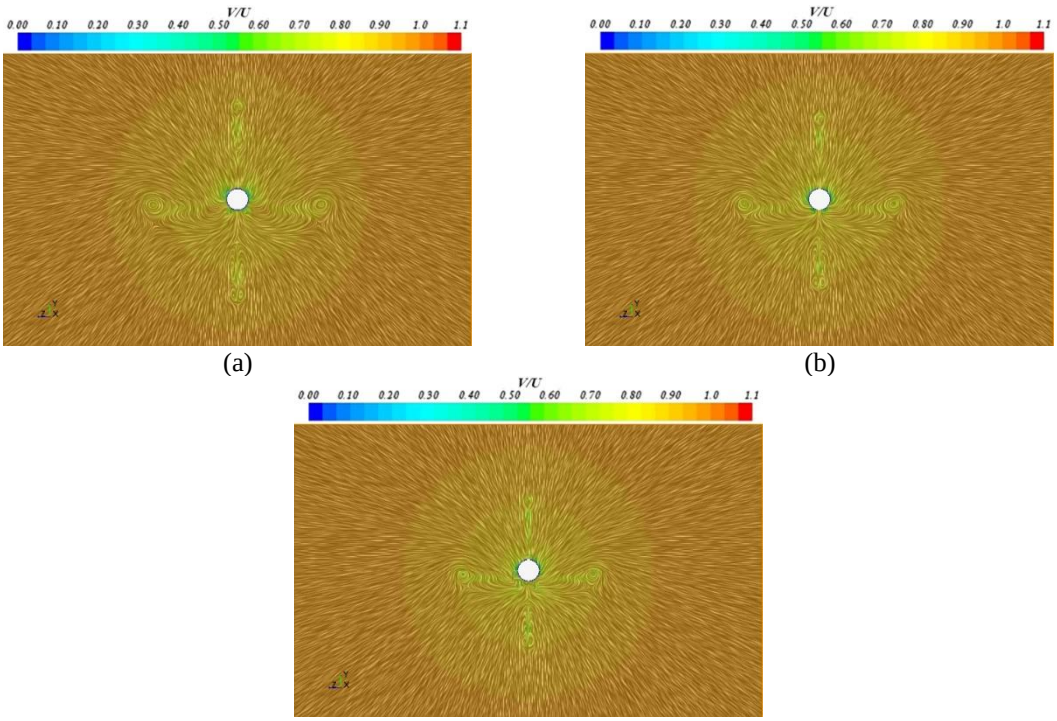

(a) (b)

(c)

Fig. 20 Comparison of the flow pattern with integrated velocity vectors at the location of submarine propeller (on the y-z plane at cross-section $X/L=0.978$) for three locations of the control surfaces with $\delta=5°$: (a) $X/L=0.89$, (b) $X/L=0.92$, (c) $X/L=0.95$

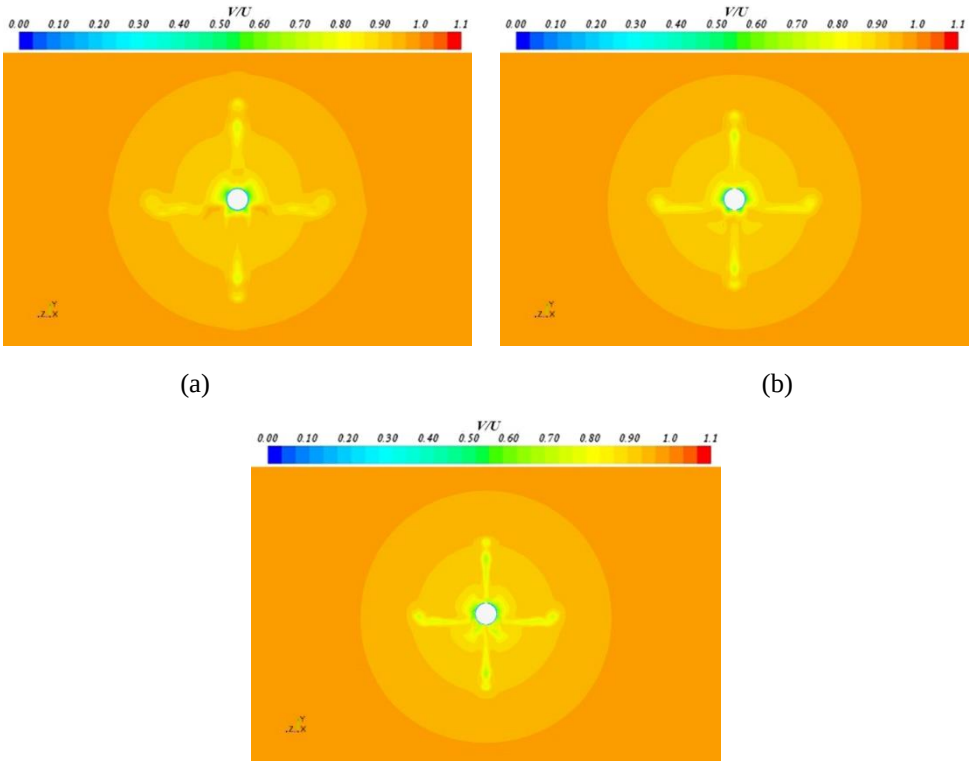

Fig. 21 Comparison of the distribution of flow average velocity on the location of the submarine propeller (on the y-z plane at the cross-section $X/L=0.978$) for three locations of the control surfaces with angle $\delta=5°$: (a) $X/L=0.89$, (b) $X/L=0.92$, (c) $X/L=0.95$

In Fig. 22, the turbulence intensity contour on the y-z plane are plotted and at a distance of $X/L=0.978$ for three locations of the stern planes, $X/L=0.89,0.92,0.95$. The surfaces located on the horizontal plane x-z has have a deflection angle of ($\delta=5°$) around the z-axis. It can be concluded that for the stern planes located at the distance of $X/L=0.89$, the highest turbulence intensity occurs near the propeller operating area. In addition, maximum turbulence intensity contour in this case has the highest width in comparison with the other two cases. For the two cases of the stern planes mounted at the distance of $X/L=0.92,0.95$, the propeller turbulence intensity is approximately the same in the propeller operating area and is not significantly different between the two states in this regard. Hence, it can be revealed that when the stern planes have a low deflection angle, it is generally better to install the stern planes at distances near the end of the heel.

In Fig. 23, the dimensionless average velocity is plotted on the y-z plane at a longitudinal distance of $X/L=1$, $Y/R=0$ and deflection angle of $\delta=5°$ around the z-axis for three locations of $X/L=0.89,0.92,0.95$. As can be seen, by moving in the transverse direction from the center of the model to the outside, the velocity diagram has an average decrease at two points, which respectively

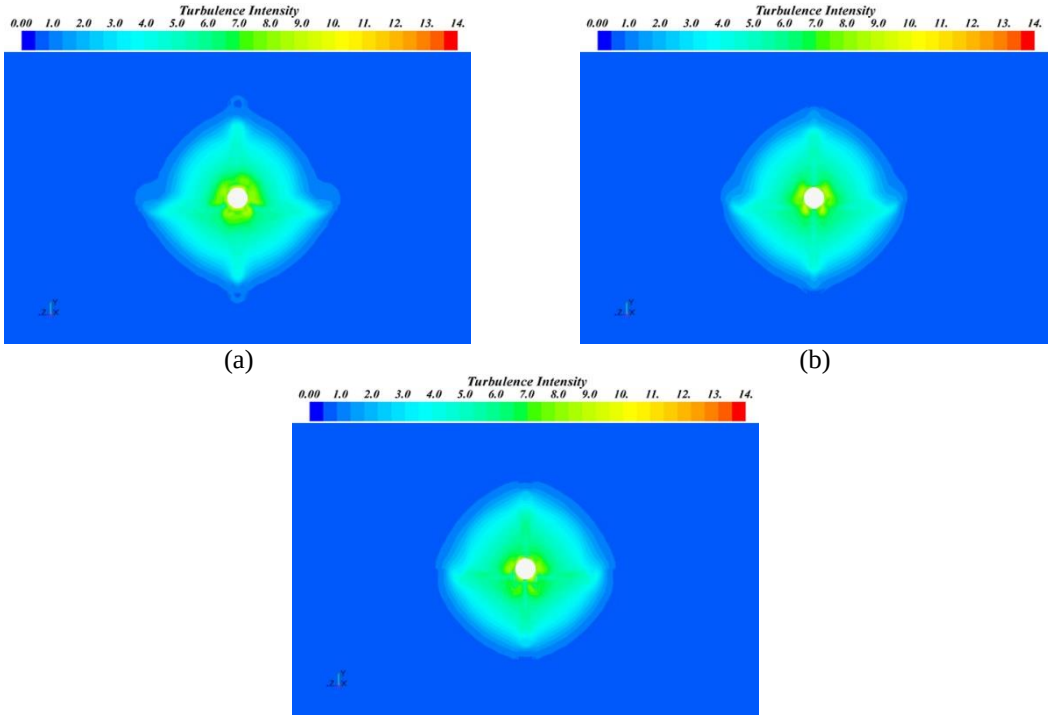

Fig. 22 Comparison of the turbulence intensity on the location of the submarine propeller (on the y-z plane at the cross-section $X/L=0.978$) for the three locations of the control surfaces with angle $\delta=5°$: (a) $X/L=0.89$, (b) $X/L=0.92$, (c) $X/L=0.95$

represents the hull wake flow, which interfere with the flow attached to the stern surface of the stern planes and the vortex flow produced from the transverse stern planes with a deviation angle of δ = 5°. Maximum average velocity decreases in the middle part. Minimum average velocity decrease belongs to the vortex flow generated from the horizontal stern planes after that it is continued horizontally. Since the main objective in improving the submarine wake flow is to improve the flow below the propeller radius, $Z/R\le 0.5$, it can be seen that wake width for $X/L=0.95$ decreases to the hull width by moving the stern planes from $X/L=0.89$ to $X/L=0.95$ in comparison with the other distances, $X/L=0.89,0.92$. As well, the average velocity in the center of the submarine model's wake flow increases. As a result, by increasing the ratio of the minimum value to the maximum flow velocity, the non-uniformity of the wake flow is reduced.

In Fig. 24, the turbulence intensity diagram on the y-z plane is plotted at $X/L=1$ and $Y/R=0$ for the three locations of the stern planes, $X/L=0.89,0.92,0.95$ and the deflection angle of $\delta=5°$. As can be seen in this figure, for the submarine model's stern planes with a deviation angle ($\delta=5°$), the turbulence intensity of each stern planes are most closely related to each other. But in terms of width, at a distance of $Z/R\le 0.5$, the graph of the distance $X/L=0.89$ is wider and the graph of the distance =0.95 is wider outside the distance.

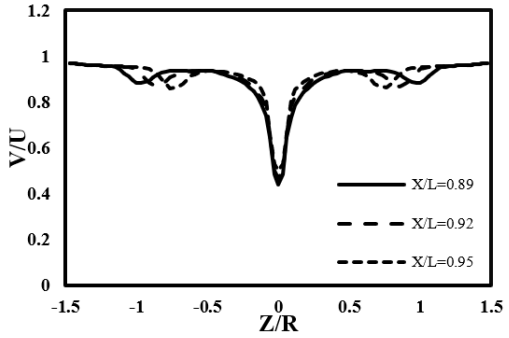

Fig. 23 Average velocity diagram in transverse direction at $Y/R=0$ from center of submarine model for three locations of stern planes and in a case where the horizontal stern planes have a $\delta=5°$ deflection angle

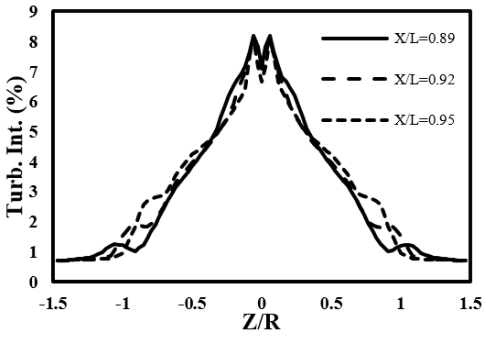

Fig. 24 Turbulence intensity diagram in transverse direction at $Y/R=0$ from center of submarine model for three locations of stern planes and in a case where the horizontal stern planes have a $\delta=5°$ deflection angle

7. Conclusions

In this study, the effect of longitudinal position of the control surfaces on the submarine stern was performed numerically. In order to investigate the effect of the longitudinal position of the control surfaces on the surrounding flow field and the submarine wake flow, these surfaces were positioned at three longitudinal distances from the end of the stern. The surrounding flow field and the wake formed at the end of the submarine were evaluated in terms of flow structure and values of turbulence velocity and intensity. The results can be summarized as follows:

- Placing the control surfaces at the stern portion of the hull causes extensive changes in the surrounding flow field and the wake flow at the downstream of the stern.
- As the control surfaces move from the nose to the stern end, the wake flow formed at the submarine end is increased; but at the same time, the elongation of the control surfaces wake flow in the stern area decreases. Thus, reducing the average velocity in the wake area due to the movement of the control surfaces toward the stern end is less than the expected value.

- By installing control surfaces at the distances closer to the end of the stern, the amount of drag force applied by the fluid to the submarine hull reduces.
- While increasing the stability of the stern planes, the installation of control surfaces near the stern end reduces also the likelihood of cavitation at the end of the stern.
- Compared to the control surfaces at lower distances, their installation near the end of the stern enhances the controllability of the submarine dramatically.
- Despite decreasing the average velocity at some points, the installation of control surfaces near the end of the stern causes the average velocity to increase at the below the radius of the submarine propeller, and consequently to reduce the non-uniformity of the propeller inlet flow.
- In terms of the turbulence intensity value at the below the radius of the submarine propeller, installation of control surfaces near the end of the stern causes the value and width of the turbulence intensity to decrease.
- Installation of control surfaces near the end of the stern allows the streamlines to enter the submarine propeller more smoothly and uniformly after crossing the surfaces.

In general, based on the results of this study, the installation of control surfaces at the distances near the end of the stern can reduce the non-uniformity of the inlet flow to the propulsion system while simultaneously can decrease the drag, improving the submarine steering capability.

Acknowledgements

The authors gratefully acknowledge the various support staff of their respective organizations who have helped make this work possible.

References

Carrica, P.M., Kim, Y. and Martin, J.E. (2019), "Near-surface self propulsion of a generic submarine in calm water and waves", *Ocean Eng*., **183**, 87-105. https://doi.org/10.1016/j.oceaneng.2019.04.082.

Dubbioso, G., Broglia, R. and Zaghi, S. (2017), "CFD analysis of turning abilities of a submarine model", *Ocean Eng*., **129**, 459-479. https://doi.org/10.1016/j.oceaneng.2016.10.046.

Fureby, C. and Norrison, D. (2019), "RANS, DES and LES of the Flow Past the 6: 1 Prolate Spheroid at 10 and 20 Angle of Incidence", in: AIAA Scitech 2019 Forum. p. 85. https://doi.org/10.2514/6.2019-0085.

Groves, N.C., Huang, T.T. and Chang, M.S. (1989), Geometric characteristics of DARPA (Defense Advanced Research Projects Agency) SUBOFF models (DTRC model numbers 5470 and 5471). David Taylor Research Center Bethesda MD Ship Hydromechanics Dept.

Huang, T., Liu, H.L., Groves, N., Forlini, T., Blanton, J., Gowing, S. and Liu, H.L. (1994), Measurements of flows over an axisymmetric body with various appendages in a wind tunnel: the DARPA SUBOFF experimental program.

Jiménez, J.M., Reynolds, R.T., Smits, A.J., JimÃŠnez, J.M., Reynolds, R.T., Smits, A.J., (2010), "The effects of fins on the intermediate wake of a submarine model", *J. Fluids Eng*., **132**, 31102. https://doi.org/10.1115/1.4001010

Liu, Z., Xiong, Y., Wang, Z., Song, W. and Tu, C. (2010), "Numerical simulation and experimental study of the new method of horseshoe vortex control", *J. Hydrodyn. Ser. B*, **22**, 572-581. https://doi.org/10.1016/S1001-6058(09)60090-1.

Liu, Z., Xiong, Y., Wang, Z., Wang, S. and Tu, C. (2011), "Experimental study on effect of a new vortex control baffler and its influencing factor", *China Ocean Eng*., **25**, 83-96. https://doi.org/10.1007/s13344-011-0007-

8.
Pan, Y., Zhang, H. and Zhou, Q. (2019), "Numerical simulation of unsteady propeller force for a submarine in straight ahead sailing and steady diving maneuver", 1-15. https://doi.org/10.1016/j.ijnaoe.2019.04.002
Posa, A. and Balaras, E. (2016), "A numerical investigation of the wake of an axisymmetric body with appendages", *J. Fluid Mech*., **792**, 470-498. https://doi.org/10.1017/jfm.2016.47.
Posa, A., Broglia, R., Felli, M., Falchi, M. and Balaras, E. (2019), "Characterization of the wake of a submarine propeller via Large-Eddy simulation", *Comput. Fluids*, **184**, 138-152. https://doi.org/10.1016/j.compfluid.2019.03.011.
Rao, Z. and Yang, C. (2017), "Numerical prediction of effective wake field for a submarine based on a hybrid approach and an RBF interpolation", *J. Hydrodyn*., **29**, 691-701. https://doi.org/10.1016/S1001-6058(16)60781-3.
Zhang, J., Zhao, F., Hong, F. and Xu, J. (2003), "Towing PIV and its application on the juncture forms of stern appendage with main-body", in: Optical Technology and Image Processing for Fluids and Solids Diagnostics 2002. International Society for Optics and Photonics, 208-213. https://doi.org/10.1117/12.509746.
Zhihua, L., Ying, X. and Chengxu, T. (2011), "Numerical simulation and control of horseshoe vortex around an appendage–body junction", J. Fluids Struct., **27**, 23-42. https://doi.org/10.1016/j.jfluidstructs.2010.08.006.

PL

Nomenclature

C_1, C_2, C_μ	Constants for turbulent model
C_f	Drag coefficient
C_p	Pressure coefficient
D	Diameter of submarine model [$\boldsymbol{m}$]
k	Turbulence kinetic energy [$\boldsymbol{m/s}$]
L	Length of submarine model [$\boldsymbol{m}$]
P	Pressure [$\boldsymbol{Pa}$]
R	Radius of submarine model [$\boldsymbol{m}$]
S	Strain rate [$\boldsymbol{1/s}$]
u	Fluctuation velocity in x direction [$\boldsymbol{m/s}$]
U_{mean}	Velocity of inlet [$\boldsymbol{m/s}$]
U	Freestream velocity upstream of the model [$\boldsymbol{m/s}$]
V	Local mean velocity of flow [$\boldsymbol{m/s}$]
v	Fluctuation velocity in y direction [$\boldsymbol{m/s}$]
X, Y, Z	Cartesian positions to the reference coordinate [$\boldsymbol{m}$]

Greek symbols

ℓ	Distance of the end of control surfaces from stern's end [$\boldsymbol{m}$]
ρ	Density [$\boldsymbol{kg/m^3}$]
ε	Turbulence kinetic energy dissipation rate [$\boldsymbol{m/s^2}$]
μ	Dynamic viscosity [$\boldsymbol{kg/(m \cdot s)}$]
μ_t	Turbulent dynamic viscosity [$\boldsymbol{kg/(m.s)}$]
υ_t	Turbulent viscosity [$\boldsymbol{m^2/s}$]
σ_k	Turbulent Prandtl number for k
σ_ε	Turbulent Prandtl number for $\boldsymbol{\varepsilon}$
σ_t	Schmidt number
Γ	Diffusion number [$\boldsymbol{m^2/s}$]
Φ	Scalar

δ	Deflection angle of control surface [°]
δ_{ij}	Kronecker delta

Subscripts

i,j	Any directions of x, y